ACS NANO
Cite This: ACS Nano XXXX, XXX, XXX−XXX
www.acsnano.org

ARTICLE

Cesium-Incorporated Triple Cation Perovskites Deliver Fully Reversible and Stable Nanoscale Voltage Response

Elizabeth M. Tennyson,[†,‡] Bart Roose,[§] Joseph L. Garrett,[‡,∥] Chen Gong,[†,‡] Jeremy N. Munday,[‡,⊥] Antonio Abate,[#,▽] and Marina S. Leite*[,†,‡]

[†]Department of Materials Science and Engineering, University of Maryland, College Park, Maryland 20742, United States
[‡]Institute for Research in Electronics and Applied Physics, University of Maryland, College Park, Maryland 20742, United States
[§]Cavendish Laboratory, Department of Physics, University of Cambridge, JJ Thomson Avenue, CB3 0HE Cambridge, United Kingdom
[∥]Department of Physics, University of Maryland, College Park, Maryland 20742, United States
[⊥]Department of Electrical and Computer Engineering, University of Maryland, College Park, Maryland 20742, United States
[#]Helmholtz-Zentrum Berlin für Materialien und Energie, Kekuléstraße 5, 12489 Berlin, Germany
[▽]Department of Chemical, Materials and Production Engineering, University of Naples Federico II, Piazzale Tecchio 80, 80125 Fuorigrotta, Naples, Italy

Supporting Information

ABSTRACT: Perovskite solar cells that incorporate small concentrations of Cs in their A-site have shown increased lifetime and improved device performance. Yet, the development of fully stable devices operating near the theoretical limit requires understanding how Cs influences perovskites' electrical properties at the nanoscale. Here, we determine how the chemical composition of three perovskites ($MAPbBr_3$, $MAPbI_3$, and Cs-mixed) affects their short- and long-term voltage stabilities, with <50 nm spatial resolution. We map an anomalous irreversible electrical signature on $MAPbBr_3$ at the mesoscale, resulting in local V_{oc} variations of ∼400 mV, and in entire grains with negative contribution to the V_{oc}. These measurements prove the necessity of high spatial resolution mapping to elucidate the fundamental limitations of this emerging material. Conversely, we capture the fully reversible voltage response of Cs-mixed perovskites, composed by $Cs_{0.06}(MA_{0.17}FA_{0.83})_{0.94}Pb(I_{0.83}Br_{0.17})_3$, demonstrating that the desired electrical output persists even at the nanoscale. The Cs-mixed material presents no spatial variation in V_{oc}, as ion motion is restricted. Our results show that the nanoscale electrical behavior of the perovskites is intimately connected to their chemical composition and macroscopic response.

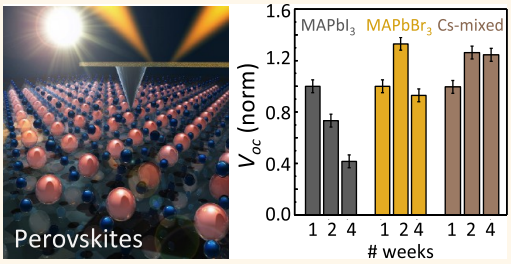

KEYWORDS: *perovskite solar cells, $MAPbI_3$, $MAPbBr_3$, Cs-mixed perovskite, ion motion, nanoscale voltage, Kelvin probe force microscopy*

The progress and research effort that has happened to improve perovskite solar cells in the past decade is immense.[1,2] This photovoltaic (PV) material class has now achieved power-conversion efficiencies (η) for both single-junction[3,4] and tandem devices containing perovskites[5] >22%. These advancements demonstrate researchers ripening comprehension of perovskites, and thus, the fabrication processes for higher quality materials, such as electronic charge carrier transport layers and film interfaces, are being refined.[6−9] While such advances are necessary to develop commercial PV devices, short- and long-term stability under realistic atmosphere environments and perovskites' inability to pass accelerated aging tests remain challenging.[10,11]

The heterogeneity and dynamics in perovskites begin at the nanoscale,[12−18] and locally revealing the primary performance parameters with high spatial resolution[19−21] can potentially be correlated to the beneficial, parasitic, and/or transient response and the overall device performance. For instance, under illumination, perovskites have local variations in open-circuit voltage (V_{oc}),[12,22,23] photocurrent,[24] and photoluminescence signal[25] as a function of both space and time. The primary

Received: September 24, 2018
Accepted: December 26, 2018
Published: December 26, 2018

DOI: 10.1021/acsnano.8b07295
ACS Nano XXXX, XXX, XXX−XXX

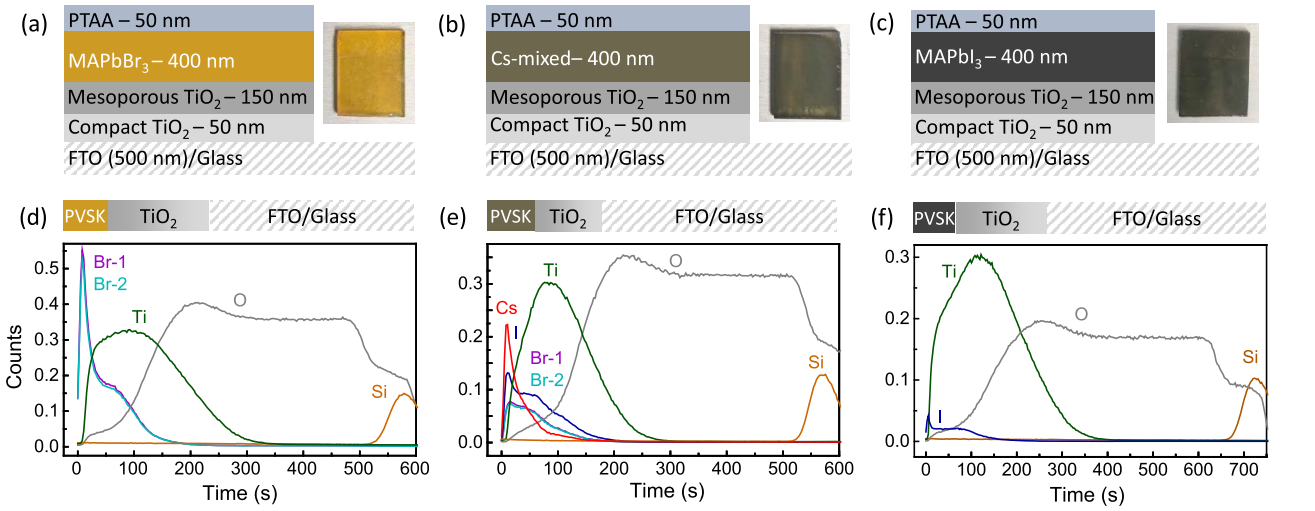

Figure 1. Chemical composition analysis of perovskites by ToF-SIMS. Schematic and real-color photographs of perovskite samples: (a) $MAPbBr_3$, (b) Cs-mixed, and (c) $MAPbI_3$. Samples size = 1.2 × 1.5 cm^2. (d–f) Representative depth profiles of ToF-SIMS measurements acquired for each sample.

culprit of the heterogeneity is still under debate, but the strongest hypothesis thus far suggests halide ion migration.[26−29] Recently, triple cation perovskites containing methylammonium (MA), formamidinium (FA), and Cs have been presented as a promising alternative, due to experimental evidence that Cs incorporation improves thermal, moisture, and photoelectrical stabilities.[30−33] Simultaneously, the devices can maintain its output η, suitable for the future, large-scale deployment of this PV material. It has been lately observed that the addition of Cs affects the structural properties of the absorbing layer by decreasing its lattice constant, while simultaneously preventing ion migration.[34,35] Nevertheless, it is currently unknown how the electrical signal of the grains constituting these perovskites changes upon illumination and if this composition suffers from ion motion processes at the nanoscale.

Here we elucidate how the crystal lattice reduction caused by the addition of Cs, MA, FA, Br, and I in triple cation perovskites leads to a fully reversible nanoscale voltage response in solar cells for both short- and long-term stabilities. By implementing fast Kelvin probe force microscopy (KPFM), we directly image nanoscale spatial variations in V_{oc} under 1 sun illumination of three perovskites with different compositions. We find that the perovskite with small concentrations of Cs yields a uniform and steady V_{oc} upon light treatment, irrespective of grains and grain boundaries. The $MAPbBr_3$ composition shows an anomalous, nonreversible light-induced electrical behavior. For this material, illumination under 1 sun results in ∼400 mV variation ranging from single grains to clusters, where >10% of the perovskite has "negative voltage" regions, with no morphological variations. Further, through spatially and temporally resolving the light-induced changes in the $MAPbBr_3$ sample, we demonstrate the effect of ion motion in these solar cells' V_{oc}, which is responsible for the observed dynamics. Our results show that the Cs-mixed perovskite is the most stable composition at both the nano- and macroscale, with uniform V_{oc} spatial distribution. We foresee our nanoscale V_{oc} measurements being expanded to other perovskites, where the role of relative humidity, oxygen, temperature, light, and bias on perovskites grains and interfaces could be deconvoluted by mapping the individual contribution of each degradation factor individually. These experiments would help elucidate the driving forces for several perovskites' degradation, currently not fully understood.

RESULTS AND DISCUSSION

Perovskite solar cells are, in most cases, formed by an organic–inorganic hybrid material blend with a chemical formula of ABX_3 (A = monovalent cation, B = inorganic cation, and X = halide anion). The constituents of this structural form have been researchers' primary tuning knob used to alter the optoelectronic properties of perovskites as well as improve the thermal, structural, and photostability.[36−38] The most common compounds for each lattice position are A-site: methylammonium ($MA = CH_3NH_3^+$), formamidinium ($FA = HC(NH_2)_2^+$) and inorganic Cs^+; B-site: Pb^{2+}, which has the best performance in this location (although very recent studies show that a partial substitution by Co^{2+} or Bi^{3+} could boost output power);[38,39] and X_3-site: I^-, Br^-, and/or Cl^-.

We investigate three perovskite thin-films with different compositions. First, the conventional $MAPbI_3$ (with bandgap = 1.58 eV) is selected because its electronic properties are well documented, and therefore, it is an ideal candidate for systematic testing of the chemical composition contribution to the nanoscale electrical response. Another pure halide, $MAPbBr_3$, is analyzed; this perovskite has a higher bandgap (2.2 eV) and, thus, larger V_{oc} and limited photocurrent, and it could be utilized in tandem PV devices. The overall electrical performance (macroscopic) of pure-halide perovskites has been observed to degrade with exposure to either light and/or moisture, and when a mixture of Br and I halides is used, photoinduced ion segregation occurs,[28] specifically when the sole A-site compound is MA.[40,41] Therefore, we implement cation engineering by adding a small amount of an inorganic component, Cs^+, to a mixture of MA and FA and also use a combination of halide atoms: $Cs_{0.06}(MA_{0.17}FA_{0.83})_{0.94}Pb(I_{0.83}Br_{0.17})_3$ (*i.e.*, Cs-mixed, also with bandgap ≈1.58 eV).[42] This approach has been observed to improve the stability in ambient environments substantially.[33] See the Methods section for detailed information about the perovskite thin-film/device fabrication steps. We fabricate half devices, composed of PTAA/perovskite/TiO_2/FTO/glass, to perform nanoscale

DOI: 10.1021/acsnano.8b07295
ACS Nano XXXX, XXX, XXX–XXX

electrical measurements through KPFM, as will be presented later in this article.

We perform time-of-flight secondary ion mass spectroscopy (ToF-SIMS) and obtain the depth profiles of the relevant elements.[43] Figure 1 displays a schematic of the perovskite samples and their corresponding thicknesses, plus the respective real color photographs (Figure 1a–c), which are an indicator of their bandgaps. The elemental depth profiles obtained by ToF-SIMS (Figure 1d–f) validate the presence of the constituent elements in the perovskite films with no diffusion throughout the other active layers of the devices, see Methods for experimental details. As desired, Br (two isotopes shown as Br-1 and Br-2 in Figure 1), Cs, and I are all confined to the perovskite layer of the samples. Further, the chemical composition is uniform at the microscale throughout each layer, as shown in Figure S1, which displays additional ToF-SIMS depth profiles, acquired at other locations of the films. This uniform distribution in the composition is further verified with the ToF-SIMS chemical maps of relevant ions for all perovskite samples, see Figures S2–S4 in the Supporting Information.

Each perovskite thin-film investigated here also has a full device counterpart. Light J–V curves and η *vs* time plots are presented in Figure 2 and Figure S5, detailing their average

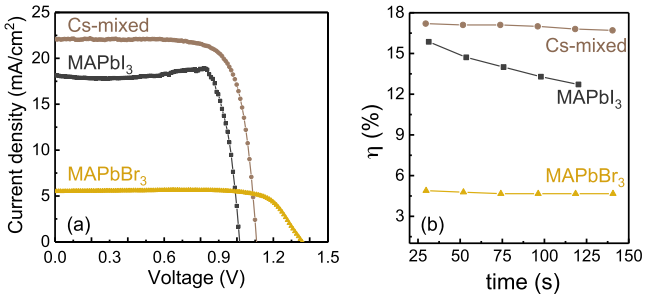

Figure 2. Macroscopic performance and short-term stability of perovskite solar cells. (a) Light J–V curves for perovskite solar cells (color coded). For Cs-mixed, $MAPbI_3$, and $MAPbBr_3$: V_{oc} = 1.11, 1.02, and 1.36 V, J_{sc} = 22.1, 18.1, and 5.5 mA/cm^2, FF = 76, 85, and 76%, and η = 18.6, 15.7, and 5.7%, respectively. (b) Power conversion efficiency (η) *vs* time for each perovskite device. The Cs-mixed sample shows the highest performance and stability, while the $MAPbI_3$ device degrades rapidly with time.

performance parameters (see Methods for parameter specification). From the macroscopic measurements, it is clear that the Cs-mixed sample has the highest η at 18.6% while concurrently having excellent short-term performance stability (Figure 2b). The $MAPbBr_3$ solar cell has the lowest efficiency at 5.7% despite having the largest V_{oc} (due to its wide bandgap) and also maintains a constant electrical output with time, see Figure 2b. Yet the $MAPbI_3$ device, which initially has a promising η = 15.7%, rapidly falls to <13% in 2 min, signifying that this composition is the least electrically stable. Furthermore, despite the larger fill factor (FF), the $MAPbI_3$ light J–V curve contains an undesirable bump between 0.8 and 0.9 V, which is attributed to charge build-up close to the electrical contacts.[44] For these reasons, we have chosen to focus our high-resolution mapping experiments on the $MAPbBr_3$ and Cs-mixed perovskite compositions, to understand how their nanoscale voltage behavior influences the materials' electrical stability.

We image the nanoscale, real-time V_{oc} response of the perovskites by KPFM under 1 sun illumination conditions and extremely low humidity. A schematic of the KPFM experimental setup is presented in Figure 3. The samples are

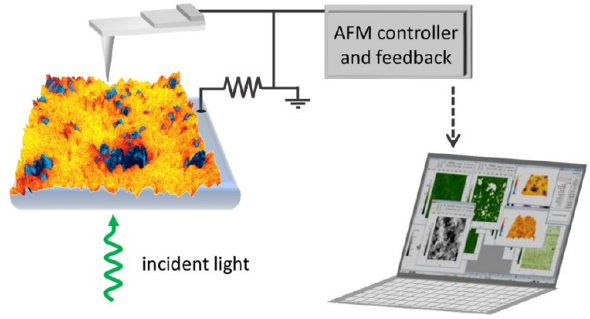

Figure 3. Imaging the V_{oc} response in perovskites at the nanoscale. Schematic of the illuminated-KPFM experimental setup, where the perovskite samples are back illuminated, and the local voltage signal is measured by an AFM probe using KPFM. Because the perovskite back contact is grounded with respect to the tip, the data acquired under illumination are proportional to the V_{oc} of the solar cell.

illuminated from the bottom using a 532 nm laser beam incident on a glass prism, which reflects an equivalent photon flux of 1 sun up toward the sample. Briefly, KPFM measures the work function difference between the atomic force microscope (AFM) probe and the sample surface.[13] Upon illumination, the perovskite absorbs photons, which generate charge carriers, introducing quasi-Fermi level splitting (directly proportional to the V_{oc}) and thus changing the work function of the material. By subtracting an illuminated KPFM scan by a dark one performed in the same location, and maintaining a common electrical ground between the probe and the perovskite sample's back electrode (FTO in this case), we image V_{oc} with spatial resolution <50 nm.[12,19] The relative humidity in the AFM chamber is held <8% (Figure S6) by continuously flowing dry air into the microscope through a piping system. See the Methods section for more details on experimental parameters. The extremely low-humidity environment, combined with the fact that all samples have a PTAA layer,[45] assures negligible perovskite hydration during the voltage scans presented here. We map the nanoscale voltage response of perovskite photovoltaic devices before, during, and after illumination, termed here $Dark_{(1)}$, Light, and $Dark_{(2)}$, respectively.

Figure 4 displays measurements of the nanoscale voltage response of the $MAPbBr_3$ perovskite under 1 sun illumination, where we find an irreversible behavior upon the material's first exposure to light. During the entirety of our experiments, no topography changes are observed (Figure 4a–d), indicating that any variations in the electrical signal are due to nonmorphological properties of the perovskites. It also demonstrates that during the scans, the AFM probe is kept intact (and all changes in tip–sample interactions are due to variations in the electrical output of the perovskites). The $MAPbBr_3$ perovskite presents extraordinary, irreversible light-induced electrical behavior at the nanoscale. Before this sample is exposed to light, the voltage is nearly uniform, see $Dark_{(1)}$ image in Figure 4e, with an average voltage equal to 1.04 V. This situation corresponds to a metastable configuration within the perovskite, as $MAPbBr_3$ is known for a high density of

DOI: 10.1021/acsnano.8b07295
ACS Nano XXXX, XXX, XXX–XXX

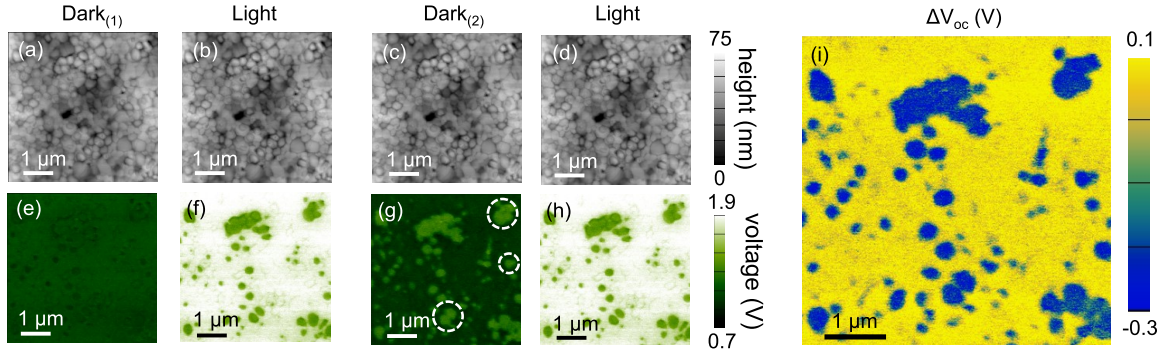

Figure 4. Nanoscale irreversible voltage response in $MAPbBr_3$ perovskites. (a–d) AFM topography maps of the $MAPbBr_3$ sample and their respective (e–h) voltage images under sequential dark and illuminated conditions. Here, despite consistent topography, an irreversible electrical process occurs within the $MAPbBr_3$ perovskite film. (i) Spatial variation in open-circuit voltage (ΔV_{oc}) under local illumination. For all measurements, relative humidity <8%, and for light-KPFM, the illumination conditions are a 532 nm laser under 1 sun incident photon flux.

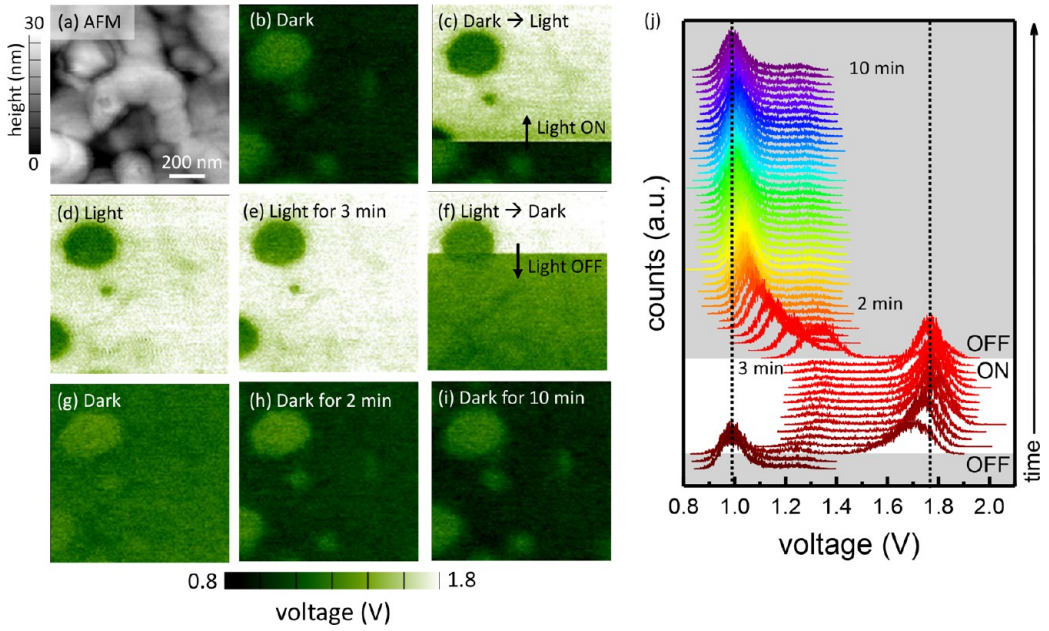

Figure 5. Dynamic, reversible electrical response after the first illumination of $MAPbBr_3$. (a) Topography map. (b–i) Fast Dark- and Light-KPFM scans (16 s/scan) shown in chronological order, demonstrating the slow reversibility of the voltage response in 10 min post-illumination. During scan (c), the 532 nm laser (at 1 sun) is turned ON, scan direction bottom → top. During scan (f), the illumination source is turned OFF, scan direction from top → bottom. (j) Corresponding voltage histograms for the entire fast KPFM series.

defects (vacancies and interstitials).[46] Upon illumination (Figure 4f), we now measure an inhomogeneous photovoltage response which differentiates itself from the distribution of the initial dark scan. After sample illumination (Figure 4g), an unexpected electrical and reversible state emerges, termed as $Dark_{(2)}$. We find two distinct regions within the $MAPbBr_3$ voltage maps in Figure 4e–h: (i) the "background", where the light-induced voltage shows the largest increase (very light green, voltage = 1.84 V), and (ii) well-defined perovskite grain and grains clusters which have become inactive photovoltage sites, viewed as the medium-green color in Figure 4f–h (voltage = 1.49 V in both cases, see regions highlighted by white dashed circles in Figure 4g). Note that after the initial illumination of the $MAPbBr_3$ sample (shown in Figure 4f), the voltage responses, both Light and Dark, become reversible (as will be discussed later). Contrarily, the $MAPbI_3$ perovskite presents uniform voltage distribution, regardless of the grain's morphology and their boundaries. Nevertheless, this perovskite is unstable, with >20% decay in power conversion efficiency in only 2 min. See Figure S7 for our nanoscale KPFM measurements of $MAPbI_3$, which were performed prior to complete material degradation. The primary difference in nanoscale voltage behavior between the two pure-halide perovskite samples is related to their distinct Pb-halide bond lengths,[46] which ultimately affects both the ingress of ions into the perovskite lattice as well as ion motion throughout the atomic structure.

To quantify the actual effect of the high- and low-voltage regions on the time dependent V_{oc} of $MAPbBr_3$, we first subtract a $Dark_{(x)}$ image from a Light-KPFM scan (*i.e.*, Figure 4f minus Figure 4e and Figure 4h minus Figure 4g), and then we subtract those resulting maps from each other, yielding Figure 4i. Two contrasting areas are immediately apparent when comparing the resulting ΔV_{oc} map (in blue and yellow), with spatial variations in V_{oc} of 400 mV. The blue regions cover approximately 12% of the scanned area. Conversely, the yellow

DOI: 10.1021/acsnano.8b07295
ACS Nano XXXX, XXX, XXX–XXX

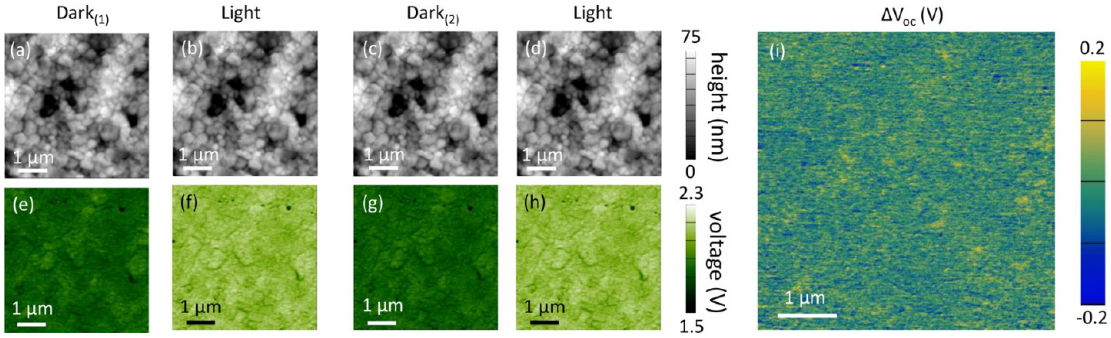

Figure 6. Nanoscale reversible voltage responses in Cs-mixed perovskites. (a–d) Topography and (e–h) Dark and light KPFM maps of the Cs-mixed sample showing fully reversible voltage and no significant spatial variations. (i) Spatial variation in open-circuit voltage (ΔV_{oc}) as a function of time under local illumination, showing uniform voltage distribution. For light-KPFM, the illumination conditions are a 532 nm laser under 1 sun incident photon flux, and all measurements held relative humidity <8%.

area corresponds to perovskite material that improved in electrical response upon light soaking (see $Dark_{(2)}$ KPFM map in Figure 4g). Surprisingly, despite the negative-voltage grains in the ΔV_{oc} map, the average value of the entire scanned region ($\langle \Delta V_{oc} \rangle$) increases by 30 mV after illumination, a significant value considering that the volume of excited carriers is extremely small (due to the focused illumination used in our experiments). Note that a macroscopic measurement would not capture such irreversible behavior in the nanoscale V_{oc} and could inadvertently lead to the conclusion that the light soaking effect imaged here is constant across grains, when this is not the full story. We hypothesize that this irreversible electrical process is caused by Br^- ion motion within the perovskite film.[47−49] Because Br is a negatively charged ion, it tends to move toward the electron transport material during operation conditions (meaning, during illumination). The movement of these ions away from the surface (*i.e.*, PTAA, the hole transport layer) is likely the reason for the observed heterogeneous V_{oc} measured here.

Through fast-KPFM we determine the immediate changes that take place in the perovskites' electrical response upon illumination in two representative regions within the scanned area of Figure 4, see Figure 5 and Figure S8. Briefly, in fast-KPFM, the real-time voltage is measured, where each map is acquired in 16 s.[22] As the laser is turned ON/OFF, we capture the transient and asymmetric voltage response of this perovskite, as displayed in the maps presented in Figure 5 and in the corresponding voltage histograms. Once the sample is illuminated under 1 sun (Figure 5c), the electrical signal changes substantially, corresponding to the photogenerated voltage. Here, the "slow" voltage increase that takes place in ∼2−3 min (red-color histograms) results from ion motion within the perovskite, as stated earlier. As the material is illuminated, the electrons fill in the existing trap states.[12] Consequently, the Br^- anions now have a preferential motion direction—away from these filled states. Upon turning the laser OFF, we observe a residual positive voltage response for ∼10 min (see gradual change in signal from Figure 5f to 5i and red to purple histograms in Figure 5j). Here, the dynamic voltage signal at open-circuit conditions results from the now reversible electron and Br^- motion. Yet, there is a hysteresis in the nanoscale voltage, where it takes more than 2× longer for the voltage to equilibrate under dark conditions. Note that this time-dependent voltage behavior could not be resolved by conventional KPFM methods, as they would not capture the short-time voltage changes. If the surface probed by KPFM would be an ETM instead (such as in a perovskite/PCBM film), one would expect the voltage signal of the post-illumination scans to be initially smaller than the voltage at equilibrium (contrary to the behavior shown in Figure 5j), as we previously reported for $MAPbI_3$.[12]

The macroscopic electrical performance and stability of solar cells, shown in Figure 2, can be traced down to their nanoscale constructs. Therefore, revealing the relevant local voltage responses will help answer the following open question: Why does Cs-incorporation significantly improve overall device efficiency and stability? Thus, we dedicate this section to the effect of cation engineering on the material at short- and long-term time scales. In Figure 6 we show the morphology (which is constant as a function of time and illumination, Figure 6a–d) and electrical signal of Cs-mixed composition at the nanoscale. We measure a very uniform voltage response (Figure 6e–h) under both dark and light conditions, irrespective of the interfaces between the grains. This is desirable for large-scale solar cell deployment and a distinct difference from the behavior of $MAPbBr_3$. The Cs-mixed sample also presents fully reversible voltage response (under the experimental conditions tested here), determined by the average zero-value ΔV_{oc} map, see Figure 6i, which is well within the line-noise level of our KPFM measurements. We further confirm the ion motion suppression in the Cs-mixed perovskite by applying fast-KPFM, shown in Figure S9. As a region consisting of several grains undergoes illumination cycling, the nanoscale voltage response is fully reversible, and it immediately changes upon turning the laser ON/OFF. It is important to reiterate that, as expected, the absolute value of the V_{oc} for the Cs-mixed sample is lower than the $MAPbBr_3$ one due to its smaller bandgap energy, see Figure 2. A comparison between $MAPbI_3$ and the Cs-mixed samples corroborates our hypothesis further. While $MAPbI_3$ displays no spatial variations in the KPFM response (see Figure S7 for representative Dark-, Light-KPFM, and ΔV_{oc} maps), it is important to emphasize that the pure halide perovskite is only metastable with respect to light and quickly decays in performance as a function of time, as presented in Figure 2b. Note that a combined analysis of the nano- and macroscopic voltage response of this material is needed to determine its overall time-dependent electrical properties. The differences in the perovskites' electrical behavior can only be attributed to their compositions, as the experimental parameters, grain morphology, and thin-film stacking layers are all similar. Through our scanning probe microscopy experiments, we

DOI: 10.1021/acsnano.8b07295
ACS Nano XXXX, XXX, XXX−XXX

elucidate that the combined presence of Cs, FA, and Br prevents the degradation of the perovskites at the nanoscale, ultimately leading to the stable macroscopic response observed in this system.[32,33]

Figure 7 shows the stability of all samples investigated here after 4 weeks of KPFM experiments. As described in other

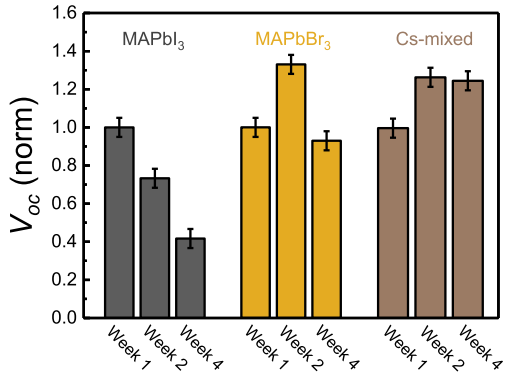

Figure 7. Analysis of perovskites' nanoscale electrical stability. Histograms of V_{oc}, extracted from the nanoscale KPFM experiments, normalized as a function of the first week for each perovskite sample. The superior long-term voltage stability of the Cs-mixed composition is evident by its steady V_{oc} signal over the course of 4 weeks.

reports,[35,42] by incorporating Cs into the A-site position (which has a smaller radius than both MA and FA), halide migration is inhibited because both MA and FA are compressed in these cases. The histograms in Figure 7 display the time dependence of the V_{oc} of all the perovskite compositions obtained by the KPFM maps, where the error bars correspond to the line-noise level of the measurements. The small increase in V_{oc} observed for both $MAPbBr_3$ and Cs-mixed after week 1 of our KPFM experiments is likely due to (i) different tip−sample interactions during the KPFM experiment (*i.e.*, fresh AFM probe used with a slightly altered work function), (ii) minor differences in optical alignment of the incident laser, (iii) variations in perovskite film thickness, as each week the sample has been imaged in another region. Even though the initial $MAPbI_3$ KPFM maps shown in Figure S7 are essentially uniform (*i.e.*, void of any defects or nonradiative recombination sites), the light-induced V_{oc} drops week-after-week, signifying material degradation. In contrast, the homogeneous voltage distribution of the Cs-mixed sample is maintained throughout the entirety of the experiments as well as its associated V_{oc}. Different than $MAPbI_3$, the Cs-mixed sample is electrically uniform at both the nano- and macroscale and has long-term stability, as presented in Figure 7. Despite the voltage heterogeneity of the $MAPbBr_3$ perovskite, the long-term electrical response stays relatively stable, although the voltage signal does show higher volatility. This phenomenon could be related to the measured irreversible electrical signal and negative-voltage sites in the $MAPbBr_3$, which in this case are likely caused by light-induced, mobile organic cation and/or bromine ions.[47,48] In comparison with the other pure halide options, the Cs-mixed perovskite has superior electrical behavior.

The significance of spatially resolving the V_{oc} of inhomogeneous materials, such as perovskites, lies in revealing changes in the optoelectronic behavior of grains and within grains related to charge carrier recombination that dominates the overall device stability and performance. To date, microscopic measurements of perovskites through scanning probe and electron microscopy-based methods have shown significant spatial variations in the photocurrent and photovoltage generated by MA and FA perovskites and are likely related to physical and chemical processes that take place once the material is exposed to ambient environment or operation conditions. In this work, we chose to image solar cell samples with identical HTM and ETM layers to ensure that all variations in signal are due to the perovskite layers, avoiding any possible influence from the carrier transport layers on the local KPFM response. Note that the band offset effect of HTM and ETM layers will be equivalent at the macroscopic and at the nanoscale as the Light- minus Dark-KPFM measurements are directly proportional to the splitting of the quasi-Fermi level of the devices. This is an advantageous feature of KPFM as a tool for directly comparing the nanoscale and macroscopic electrical behavior of the perovskites. The precise effect of specific materials on the nanoscale V_{oc} could be assessed by performing comparative analyses on devices with different HTM and ETM materials (*e.g.*, PTAA *versus* Spiro-OMeTAD, and PCBM *versus* mesoporous TiO_2 with distinct geometries).[50] Further, elucidating the voltage response of emerging perovskite materials, such as $(RbCsMAFA)PbI_3$ and Bi-halide double perovskites,[51] is critical to identify which chemical compositions can be implemented as solar cell modules. Ultimately, unravelling the driving forces for material degradation upon exposure to light (in this case), moisture, oxygen, temperature, and bias from the macro- to the nanoscale will advance the understanding of what triggers the dynamic response commonly observed in perovskites.

CONCLUSIONS

We determined the influence of chemical composition on the nanoscale, time-dependent V_{oc} for three types of perovskites: $MAPbI_3$, $MAPbBr_3$, and Cs-mixed. By performing KPFM imaging under 1 sun illumination conditions, we discovered an irreversible photovoltage response within the $MAPbBr_3$ perovskite, demonstrating the need for high spatial resolution mapping. Regions of negative-photovoltage coexist with "active" areas upon material illumination, resulting in local, spatial variations in V_{oc} of approximately 400 mV. The $MAPbI_3$ conventional perovskite presented the lowest stability among the three compositions at multiple time scales. Meanwhile, we measured a fully reversible and uniform V_{oc} response in Cs-mixed perovskites, which is due to the suppression of ion motion resulting from crystal lattice shrinkage.[52] The differences between the three samples' V_{oc} behavior are related to the occurrence and suppression of ion migration: as small concentrations of Cs are incorporated into the perovskite lattice, the movement of ions is inhibited due to strain. As a result, the nanoscale V_{oc} is homogeneous at the length scale of individual grains. Yet, for the $MAPbBr_3$ perovskite, the motion of Br^- ions causes a hysteresis on the V_{oc} response as a function of illumination.

Our nanoscale, time-dependent V_{oc} imaging/analysis can be expanded to probe the real-time response of emerging perovskites, including options for multijunction solar cells[5] and light-emitting devices. For instance, by implementing fast-KPFM, one can identify the role of different atmospheres, such as N_2, O_2, and H_2O, as well as of temperature and bias, on the dynamic electrical properties of these materials (including their combined effects). Moreover, the KPFM measurements can be

DOI: 10.1021/acsnano.8b07295
ACS Nano XXXX, XXX, XXX−XXX

combined with other AFM-based methods, such as photoconductive-AFM,[24] to provide a complete picture of the electrical (voltage and current) characteristics of the perovskites. As the search for reliable perovskites accelerates, defining the chemical compositions that lead to stable devices is key for the future deployment of high-performance and low-cost optoelectronics based on this class of material. Resolving the individual contributions of the nanoscale constructs within perovskites to the overall material behavior by time-dependent microscopic methods will enable the complete understanding of the relevant processes responsible for the solar cell's prominent dynamic response.

METHODS

Solar Cell Fabrication. Fluorine-doped tin oxide-coated glass slides (Sigma-Aldrich, 7Ω/□) were cleaned by sonication in 2% Hellmanex solution for 15 min. After rinsing with deionized water and ethanol, the substrates were again sonicated with isopropanol for 15 min and rinsed with acetone. The substrates were treated with UV-ozone for 5 min, and a 50 nm-thick TiO_2 electron selective layer was deposited by spray pyrolysis at 450 °C from a precursor solution of titanium diisopropoxide bis(acetylacetonate) (0.6 mL) and acetylacetone (0.4 mL) in anhydrous ethanol (9 mL). After the spraying, the substrates were left at 450 °C for 30 min and left to cool down to room temperature. Mesoporous TiO_2 films were spin-coated (4000 rpm, 20 s) from a 1:10 solution of TiO_2 paste (30 NR-D, Dyesol) in anhydrous ethanol. The films were annealed on a programmable hot plate (2000 W, Harry Gestigkeit GmbH) using a 45 min ramp to 450 °C, followed by a dwell time of 30 min. Perovskite films were deposited from a precursor solution; $MAPbBr_3$: MABr (1.2 M) and $PbBr_2$ (1.2 M) in anhydrous DMF:DMSO 4:1 (v:v); $MAPbI_3$: MAI (1.2 M) and PbI_2 (1.2 M) in DMSO; $Cs_{0.06}(MA_{0.17}FA_{0.83})_{0.94}Pb(I_{0.83}Br_{0.17})_3$: FAI (1 M), PbI_2 (1.1 M), MABr (0.2 M), $PbBr_2$ (0.2 M), and CsI (0.075 M) in anhydrous DMF:DMSO 4:1 (v:v). The perovskite solution was spin-coated in a two-step program at 1000 and 6000 rpm for 10 and 20 s, respectively. During the second step, 100 μL of chlorobenzene was poured onto the spinning substrate 5 s prior the end of the program. The substrates were then annealed at 100 °C for 1 h in a N_2 glovebox. Subsequently, the substrates were cooled down for a few minutes, and a PTAA (EM Index) solution (10 mg/mL in chlorobenzene) doped with bis(trifluoromethylsulfonyl)-imide lithium salt (Li-TFSI, Aldrich) and 4-*tert*-butylpyridine (TBP, Aldrich) was spun at 4000 rpm for 20 s, as according to the literature.[53] For the solar cells, 80 nm of Au was thermally evaporated under high vacuum for the top contact of the devices.

Macroscopic Light *J*–*V* Measurements. For the power conversion efficiency measurements, a solar simulator from ABET Technologies (Model 11016 Sun 2000) with a xenon arc lamp was used, and the solar cell response was recorded using a Metrohm PGSTAT302N Autolab. The intensity of the solar simulator was calibrated to 100 mW/cm^2 using a Si reference cell from ReRa Solutions (KG5 filtered). *J*–*V* curves were measured in ambient environment at room temperature and under reverse bias (from high to low voltages) conditions, at a scan rate of 10 mV/s. The active area of the cells was 0.09 cm^2, and cells were measured 2 days after their preparation.

ToF-SIMS Characterization. Using a focused Ga^+ ion beam as both primary and sputtering beam and scanning electron microscope dual-beam system, we obtained the depth profiles presented in Figure 1. Both the positive and negative secondary ions were generated by ionizing the species from the sample using a 20 keV Ga^+ ion beam with current at ∼1.1 nA. The ToF-SIMS signals were recorded by a mass spectrometer. During the measurements, the vacuum level was kept below 10^{-4} Torr at all times. Three distinct locations were measured for each perovskite sample for statistical purposes. Areas of 20 × 20 μm^2 were sputtered, while 10 × 10 μm^2 central regions were analyzed to avoid any edge effect. All ToF-SIMS maps were built using frames 2–40 in each set of measurements for similar depth within each perovskite sample, where frame 0 refers to the surface of each films.

KPFM Experiments. The KPFM measurements were performed using an atomic force microscope (AFM). We used a conductive Pt-coated Si probe with a 35 nm tip to measure the work function difference and topography of each sample simultaneously. Due to the geometry of the perovskite half-devices, in all cases we scanned the surface of the 50 nm-thick PTAA hole transport layer. To neglect the influence of moisture during the KPFM measurements, we fed piping connected to a dry air source into the AFM chamber, which maintained a humidity level within the microscope to <8% relative humidity, see Figure S6. We illuminated the sample with a power-tunable 532 nm laser (1 sun), directed into the AFM. A small glass prism was placed underneath the perovskite thin film and reflected light up toward the sample, producing a spot with 0.5 mm in diameter. Heterodyne-KPFM mode was implemented during the experiment, which measures the contact potential difference (V_{CPD}) of the tip–sample at the second resonance of the cantilever; see refs 12 and 22 for details. The line-noise of 50 mV was quantified by examining voltage line profiles. Between experiments, the perovskite samples were stored in a low-humidity desiccant chamber, with the average humidity level <10%.

ASSOCIATED CONTENT

Supporting Information

The Supporting Information is available free of charge on the ACS Publications website at DOI: 10.1021/acsnano.8b07295.

Additional TOF-SIMS depth profiles, map, and fast-KPFM scans on $MAPbBr_3$. A plot of humidity level during KPFM experiment, light and dark KPFM results for the $MAPbI_3$ perovskite film, and fast-KPFM results on the Cs-mixed sample (PDF)

AUTHOR INFORMATION

Corresponding Author

*E-mail: mleite@umd.edu.

ORCID

Elizabeth M. Tennyson: 0000-0003-0071-8445
Bart Roose: 0000-0002-0972-1475
Joseph L. Garrett: 0000-0001-8265-0661
Chen Gong: 0000-0003-3302-7675
Jeremy N. Munday: 0000-0002-0881-9876
Marina S. Leite: 0000-0003-4888-8195

Notes

The authors declare no competing financial interest.

ACKNOWLEDGMENTS

M.S.L. acknowledges the financial support from the National Science Foundation (ECCS-1610833), the 2016 APS Ovshinsky Sustainable Energy Fellowship, and the 2015 RASA/UMD award. E.M.T. and M.S.L. thank the 2017/2018 Hulka Energy Research Fellowship, the 2017/2018 All-S.T.A.R. Fellowship, the 2017 Graduate Student Summer Research Fellowship, and the 2016/2017 Dean's Dissertation Fellowship. C.G. and M.S.L. thank the 2017 Graduate Student Summer Research Fellowship. J.L.G. and J.N.M. acknowledge funding from the UMD Department of Physics through The Thomas Mason Interdisciplinary Physics Fund. We also thank the infrastructure of the Maryland Nanocenter and its AIMLab and FABLab.

DOI: 10.1021/acsnano.8b07295
ACS Nano XXXX, XXX, XXX–XXX

REFERENCES

(1) Correa-Baena, J.-P.; Saliba, M.; Buonassisi, T.; Grätzel, M.; Abate, A.; Tress, W.; Hagfeldt, A. Promises and Challenges of Perovskite Solar Cells. *Science* **2017**, *358*, 739−744.

(2) Hoye, R. L. Z.; Schulz, P.; Schelhas, L. T.; Holder, A. M.; Stone, K. H.; Perkins, J. D.; Vigil-Fowler, D.; Siol, S.; Scanlon, D. O.; Zakutayev, A.; Walsh, A.; Smith, I. C.; Melot, B. C.; Kurchin, R. C.; Wang, Y.; Shi, J.; Marques, F. C.; Berry, J. J.; Tumas, W.; Lany, S.; et al. Perovskite-Inspired Photovoltaic Materials: Toward Best Practices in Materials Characterization and Calculations. *Chem. Mater.* **2017**, *29*, 1964−1988.

(3) Yang, W. S.; Park, B.-W.; Jung, E. H.; Jeon, N. J.; Kim, Y. C.; Lee, D. U.; Shin, S. S.; Seo, J.; Kim, E. K.; Noh, J. H.; Seok, S. I. Iodide Management in Formamidinium-Lead-Halide−Based Perovskite Layers for Efficient Solar Cells. *Science* **2017**, *356*, 1376−1379.

(4) Green, M. A.; Hishikawa, Y.; Warta, W.; Dunlop, E. D.; Levi, D. H.; Hohl-Ebinger, J.; Ho-Baillie, A. W. H. Solar Cell Efficiency Tables (Version 50). *Prog. Photovoltaics* **2017**, *25*, 668−676.

(5) Wu, Y.; Yan, D.; Peng, J.; Duong, T.; Wan, Y.; Phang, S. P.; Shen, H.; Wu, N.; Barugkin, C.; Fu, X.; Surve, S.; Grant, D.; Walter, D.; White, T. P.; Catchpole, K. R.; Weber, K. J. Monolithic Perovskite/Silicon-Homojunction Tandem Solar Cell with over 22% Efficiency. *Energy Environ. Sci.* **2017**, *10*, 2472−2479.

(6) Peng, J.; Wu, Y.; Ye, W.; Jacobs, D. A.; Shen, H.; Fu, X.; Wan, Y.; Duong, T.; Wu, N.; Barugkin, C.; Nguyen, H. T.; Zhong, D.; Li, J.; Lu, T.; Liu, Y.; Lockrey, M. N.; Weber, K. J.; Catchpole, K. R.; White, T. P. Interface Passivation using Ultrathin Polymer-Fullerene Films for High-Efficiency Perovskite Solar Cells with Negligible Hysteresis. *Energy Environ. Sci.* **2017**, *10*, 1792−1800.

(7) Wang, Z.; Lin, Q.; Chmiel, F. P.; Sakai, N.; Herz, L. M.; Snaith, H. J. Efficient Ambient-Air-Stable Solar Sells with 2D−3D Heterostructured Butylammonium-Caesium-Formamidinium Lead Halide Perovskites. *Nat. Energy* **2017**, *2*, 17135.

(8) He, M.; Li, B.; Cui, X.; Jiang, B.; He, Y.; Chen, Y.; O'Neil, D.; Szymanski, P.; Ei-Sayed, M. A.; Huang, J.; Lin, Z. Meniscus-Assisted Solution Printing of Large-Grained Perovskite Films for High-Efficiency Solar Cells. *Nat. Commun.* **2017**, *8*, 16045.

(9) Zhang, J.; Xu, B.; Yang, L.; Mingorance, A.; Ruan, C.; Hua, Y.; Wang, L.; Vlachopoulos, N.; Lira-Cantú, M.; Boschloo, G.; Hagfeldt, A.; Sun, L.; Johansson, E. M. J. Incorporation of Counter Ions in Organic Molecules: New Strategy in Developing Dopant-Free Hole Transport Materials for Efficient Mixed-Ion Perovskite Solar Cells. *Adv. Energy Mater.* **2017**, *7*, 1602736.

(10) Howard, J. M.; Tennyson, E. M.; Neves, B. R. A.; Leite, M. S. Machine Learning for Perovskites' Reap-Rest-Recovery Cycle. *Joule* **2019**, DOI: 10.1016/j.joule.2018.11.010.

(11) Asghar, M. I.; Zhang, J.; Wang, H.; Lund, P. D. Device Stability of Perovskite Solar Cells − A Review. *Renewable Sustainable Energy Rev.* **2017**, *77*, 131−146.

(12) Garrett, J. L.; Tennyson, E. M.; Hu, M.; Huang, J.; Munday, J. N.; Leite, M. S. Real-Time Nanoscale Open-Circuit Voltage Dynamics of Perovskite Solar Cells. *Nano Lett.* **2017**, *17*, 2554−2560.

(13) Tennyson, E. M.; Gong, C.; Leite, M. S. Imaging Energy Harvesting and Storage Systems at the Nanoscale. *ACS Energy Lett.* **2017**, *2*, 2761−2777.

(14) Tennyson, E. M.; Howard, J. M.; Leite, M. S. Mesoscale Functional Imaging of Materials for Photovoltaics. *ACS Energy Lett.* **2017**, *2*, 1825−1834.

(15) Bergmann, V. W.; Weber, S. A. L.; Javier Ramos, F.; Nazeeruddin, M. K.; Grätzel, M.; Li, D.; Domanski, A. L.; Lieberwirth, I.; Ahmad, S.; Berger, R. Real-Space Observation of Unbalanced Charge Distribution Inside a Perovskite-Sensitized Solar Cell. *Nat. Commun.* **2014**, *5*, 5001.

(16) Weber, S. A. L.; Hermes, I. M.; Turren-Cruz, S.-H.; Gort, C.; Bergmann, V. W.; Gilson, L.; Hagfeldt, A.; Graetzel, M.; Tress, W.; Berger, R. How the Formation of Interfacial Charge Causes Hysteresis in Perovskite Solar Cells. *Energy Environ. Sci.* **2018**, *11*, 2404−2413.

(17) Gu, K. L.; Zhou, Y.; Morrison, W. A.; Park, K.; Park, S.; Bao, Z. Nanoscale Domain Imaging of All-Polymer Organic Solar Cells by Photo-Induced Force Microscopy. *ACS Nano* **2018**, *12*, 1473−1481.

(18) Collins, L.; Ahmadi, M.; Wu, T.; Hu, B.; Kalinin, S. V.; Jesse, S. Breaking the Time Barrier in Kelvin Probe Force Microscopy: Fast Free Force Reconstruction Using the G-Mode Platform. *ACS Nano* **2017**, *11*, 8717−8729.

(19) Tennyson, E. M.; Garrett, J. L.; Frantz, J. A.; Myers, J. D.; Bekele, R. Y.; Sanghera, J. S.; Munday, J. N.; Leite, M. S. Nanoimaging of Open-Circuit Voltage in Photovoltaic Devices. *Adv. Energy Mater.* **2015**, *5*, 1501142.

(20) Schulz, F.; Ritala, J.; Krejčí, O.; Seitsonen, A. P.; Foster, A. S.; Liljeroth, P. Elemental Identification by Combining Atomic Force Microscopy and Kelvin Probe Force Microscopy. *ACS Nano* **2018**, *12*, 5274−5283.

(21) Fuchs, F.; Caffy, F.; Demadrille, R.; Mélin, T.; Grévin, B. High-Resolution Kelvin Probe Force Microscopy Imaging of Interface Dipoles and Photogenerated Charges in Organic Donor−Acceptor Photovoltaic Blends. *ACS Nano* **2016**, *10*, 739−746.

(22) Garrett, J. L.; Munday, J. N. Fast, High-Resolution Surface Potential Measurements in Air with Heterodyne Kelvin Probe Force Microscopy. *Nanotechnology* **2016**, *27*, 245705.

(23) Leblebici, S. Y.; Leppert, L.; Li, Y.; Reyes-Lillo, S. E.; Wickenburg, S.; Wong, E.; Lee, J.; Melli, M.; Ziegler, D.; Angell, D. K.; Ogletree, D. F.; Ashby, P. D.; Toma, F. M.; Neaton, J. B.; Sharp, I. D.; Weber-Bargioni, A. Facet-Dependent Photovoltaic Efficiency Variations in Single Grains of Hybrid Halide Perovskite. *Nat. Energy* **2016**, *1*, 16093.

(24) Kutes, Y.; Zhou, Y.; Bosse, J. L.; Steffes, J.; Padture, N. P.; Huey, B. D. Mapping the Photoresponse of $CH_3NH_3PbI_3$ Hybrid Perovskite Thin Films at the Nanoscale. *Nano Lett.* **2016**, *16*, 3434−3441.

(25) deQuilettes, D. W.; Zhang, W.; Burlakov, V. M.; Graham, D. J.; Leijtens, T.; Osherov, A.; Bulovic, V.; Snaith, H. J.; Ginger, D. S.; Stranks, S. D. Photo-Induced Halide Redistribution in Organic-Inorganic Perovskite Films. *Nat. Commun.* **2016**, *7*, 11683.

(26) Eames, C.; Frost, J. M.; Barnes, P. R. F.; O'Regan, B. C.; Walsh, A.; Islam, M. S. Ionic Transport in Hybrid Lead Iodide Perovskite Solar Cells. *Nat. Commun.* **2015**, *6*, 7497.

(27) Yoon, S. J.; Draguta, S.; Manser, J. S.; Sharia, O.; Schneider, W. F.; Kuno, M.; Kamat, P. V. Tracking Iodide and Bromide Ion Segregation in Mixed Halide Lead Perovskites During Photo-irradiation. *ACS Energy Lett.* **2016**, *1*, 290−296.

(28) Yoon, S. J.; Kuno, M.; Kamat, P. V. Shift Happens. How Halide Ion Defects Influence Photoinduced Segregation in Mxed Halide Perovskites. *ACS Energy Lett.* **2017**, *2*, 1507−1514.

(29) Li, Z.; Xiao, C.; Yang, Y.; Harvey, S. P.; Kim, D. H.; Christians, J. A.; Yang, M.; Schulz, P.; Nanayakkara, S. U.; Jiang, C.-S.; Luther, J. M.; Berry, J. J.; Beard, M. C.; Al-Jassim, M. M.; Zhu, K. Extrinsic Ion Migration in Perovskite Solar Cells. *Energy Environ. Sci.* **2017**, *10*, 1234−1242.

(30) Howard, J. M.; Tennyson, E. M.; Barik, S.; Szostak, R.; Waks, E.; Toney, M. F.; Nogueira, A. F.; Neves, B. R. A.; Leite, M. S. Humidity-Induced Photoluminescence Hysteresis in Variable Cs/Br Ratio Hybrid Perovskites. *J. Phys. Chem. Lett.* **2018**, *9*, 3463−3469.

(31) Ma, Q.; Huang, S.; Chen, S.; Zhang, M.; Lau, C. F. J.; Lockrey, M. N.; Mulmudi, H. K.; Shan, Y.; Yao, J.; Zheng, J.; Deng, X.; Catchpole, K.; Green, M. A.; Ho-Baillie, A. W. Y. The Effect of Stoichiometry on the Stability of Inorganic Cesium Lead Mixed-Halide Perovskites Solar Cells. *J. Phys. Chem. C* **2017**, *121*, 19642−19649.

(32) Hu, Y.; Aygüler, M. F.; Petrus, M. L.; Bein, T.; Docampo, P. Impact of Rubidium and Cesium Cations on the Mmoisture Stability of Multiple-Cation Mixed-Halide Perovskites. *ACS Energy Lett.* **2017**, *2*, 2212−2218.

(33) Lee, J.-W.; Kim, D.-H.; Kim, H.-S.; Seo, S.-W.; Cho, S. M.; Park, N.-G. Formamidinium and Cesium Hybridization for Photo- and Moisture-Stable Perovskite Solar Cell. *Adv. Energy Mater.* **2015**, *5*, 1501310.

DOI: 10.1021/acsnano.8b07295
ACS Nano XXXX, XXX, XXX−XXX

(34) Matsui, T.; Seo, J.-Y.; Saliba, M.; Zakeeruddin, S. M.; Grätzel, M. Room-Temperature Formation of Highly Crystalline Multication Perovskites for Efficient, Low-Cost Solar Cells. *Adv. Mater.* **2017**, *29*, 1606258.
(35) Li, Z.; Yang, M.; Park, J.-S.; Wei, S.-H.; Berry, J. J.; Zhu, K. Stabilizing Perovskite Structures by Tuning Tolerance Factor: Formation of Formamidinium and Cesium Lead Iodide Solid-State Alloys. *Chem. Mater.* **2016**, *28*, 284−292.
(36) Li, L.; Liu, N.; Xu, Z.; Chen, Q.; Wang, X.; Zhou, H. Precise Composition Tailoring of Mixed-Cation Hybrid Perovskites for Efficient Solar Cells by Mixture Design Methods. *ACS Nano* **2017**, *11*, 8804−8813.
(37) Slotcavage, D. J.; Karunadasa, H. I.; McGehee, M. D. Light-Induced Phase Segregation in Halide-Perovskite Absorbers. *ACS Energy Lett.* **2016**, *1*, 1199−1205.
(38) Klug, M. T.; Osherov, A.; Haghighirad, A. A.; Stranks, S. D.; Brown, P. R.; Bai, S.; Wang, J. T. W.; Dang, X.; Bulovic, V.; Snaith, H. J.; Belcher, A. M. Tailoring Metal Halide Perovskites Through Metal Substitution: Influence on Photovoltaic and Material Properties. *Energy Environ. Sci.* **2017**, *10*, 236−246.
(39) Hu, Y.; Bai, F.; Liu, X.; Ji, Q.; Miao, X.; Qiu, T.; Zhang, S. Bismuth Incorporation Stabilized α-$CsPbI_3$ for Fully Inorganic Perovskite Solar Cells. *ACS Energy Lett.* **2017**, *2*, 2219−2227.
(40) Yang, S.; Fu, W.; Zhang, Z.; Chen, H.; Li, C.-Z. Recent Advances in Perovskite Solar Cells: Efficiency, Stability and Lead-Free Perovskite. *J. Mater. Chem. A* **2017**, *5*, 11462−11482.
(41) Berhe, T. A.; Su, W.-N.; Chen, C.-H.; Pan, C.-J.; Cheng, J.-H.; Chen, H.-M.; Tsai, M.-C.; Chen, L.-Y.; Dubale, A. A.; Hwang, B.-J. Organometal Halide Perovskite Solar Cells: Degradation and Stability. *Energy Environ. Sci.* **2016**, *9*, 323−356.
(42) McMeekin, D. P.; Sadoughi, G.; Rehman, W.; Eperon, G. E.; Saliba, M.; Hörantner, M. T.; Haghighirad, A.; Sakai, N.; Korte, L.; Rech, B.; Johnston, M. B.; Herz, L. M.; Snaith, H. J. A Mixed-Cation Lead Mixed-Halide Perovskite Absorber for Tandem Solar Cells. *Science* **2016**, *351*, 151−155.
(43) Harvey, S. P.; Li, Z.; Christians, J. A.; Zhu, K.; Luther, J. M.; Berry, J. J. Probing Perovskite Inhomogeneity beyond the Surface: TOF-SIMS Analysis of Halide Perovskite Photovoltaic Devices. *ACS Appl. Mater. Interfaces* **2018**, *10*, 28541−28552.
(44) Tress, W.; Marinova, N.; Moehl, T.; Zakeeruddin, S. M.; Nazeeruddin, M. K.; Gratzel, M. Understanding the Rate-Dependent J-V Hysteresis, Slow Time Component, and Aging in $CH_3NH_3PbI_3$ Perovskite Solar Cells: The Role of a Compensated Electric Field. *Energy Environ. Sci.* **2015**, *8*, 995−1004.
(45) Yang, J.; Siempelkamp, B. D.; Liu, D.; Kelly, T. L. Investigation of $CH_3NH_3PbI_3$ Degradation Rates and Mechanisms in Controlled Humidity Environments using *In situ* Techniques. *ACS Nano* **2015**, *9*, 1955−1963.
(46) Lin, C.; Li, S.; Zhang, W.; Shao, C.; Yang, Z. Effect of Bromine Substitution on the Ion Migration and Optical Absorption in $MAPbI_3$ Perovskite Solar Cells: The First-Principles Study. *ACS Appl. Energy Mater.* **2018**, *1*, 1374−1380.
(47) Azpiroz, J. M.; Mosconi, E.; Bisquert, J.; De Angelis, F. Defect Migration in Methylammonium Lead Iodide and Its Role in Perovskite Solar Cell Operation. *Energy Environ. Sci.* **2015**, *8*, 2118−2127.
(48) Ghosh, S.; Pal, S. K.; Karki, K. J.; Pullerits, T. Ion Migration Heals Trapping Centers in $CH_3NH_3PbBr_3$ Perovskite. *ACS Energy Lett.* **2017**, *2*, 2133−2139.
(49) Tirmzi, A. M.; Dwyer, R. P.; Hanrath, T.; Marohn, J. A. Coupled Slow and Fast Charge Dynamics in Cesium Lead Bromide Perovskite. *ACS Energy Lett.* **2017**, *2*, 488−496.
(50) Noh, M. F. M.; Teh, C. H.; Daik, R.; Lim, E. L.; Yap, C. C.; Ibrahim, M. A.; Ahmad Ludin, N.; Mohd Yusoff, A. R. b.; Jang, J.; Mat Teridi, M. A. The Architecture of the Electron Transport Layer for a Perovskite Solar Cell. *J. Mater. Chem. C* **2018**, *6*, 682−712.
(51) Slavney, A. H.; Leppert, L.; Bartesaghi, D.; Gold-Parker, A.; Toney, M. F.; Savenije, T. J.; Neaton, J. B.; Karunadasa, H. I. Defect-Induced Band-Edge Reconstruction of a Bismuth-Halide Double Perovskite for Visible-Light Absorption. *J. Am. Chem. Soc.* **2017**, *139*, 5015−5018.
(52) Sutter-Fella, C. M.; Ngo, Q. P.; Cefarin, N.; Gardner, K. L.; Tamura, N.; Stan, C. V.; Drisdell, W. S.; Javey, A.; Toma, F. M.; Sharp, I. D. Cation-Dependent Light-Induced Halide Demixing in Hybrid Organic−Inorganic Perovskites. *Nano Lett.* **2018**, *18*, 3473−3480.
(53) Saliba, M.; Matsui, T.; Domanski, K.; Seo, J.-Y.; Ummadisingu, A.; Zakeeruddin, S. M.; Correa-Baena, J.-P.; Tress, W. R.; Abate, A.; Hagfeldt, A.; Grätzel, M. Incorporation of Rubidium Cations into Perovskite Solar Cells Improves Photovoltaic Performance. *Science* **2016**, *354*, 206−209.

DOI: 10.1021/acsnano.8b07295
ACS Nano XXXX, XXX, XXX−XXX